Microchimica Acta (2022) 189: 364
https://doi.org/10.1007/s00604-022-05453-9

ORIGINAL PAPER

Straw-sheaf–like Co_3O_4 for preparation of an electrochemical non-enzymatic glucose sensor

Muhammad Hilal[1] · Wanfeng Xie[1,2] · Woochul Yang[1]

Received: 12 May 2022 / Accepted: 9 August 2022 / Published online: 1 September 2022

Abstract

3D straw-sheaf–like cobalt oxide (SS-Co_3O_4) was prepared via the hydrothermal method and inert gas calcination of precursors without the assistance of any template or surfactant. It was composed of numerous nanoneedles with a length of ~ 8 μm and a diameter of ~ 30 nm strongly tied in the center. The SS-Co_3O_4 exhibited high crystallinity, a large surface area (39.01 $m^2.g^{-1}$), a smaller pore size (6 nm), and lower charge transfer resistance (R_{ct} = 9.35 Ω) at the electrode/electrolyte interface. A non-enzymatic glucose oxidizing electrode fabricated with SS-Co_3O_4 showed a high sensitivity (669 μA.mM^{-1}.cm^{-2}), wide linear range (0.04–4.85 mM), low limit of detection (0.31 μM), good selectivity, fast response time (5 s), and high reproducibility with a relative standard deviation of 2.25%. In addition, its robust structure demonstrated excellent electrochemical stability by retaining 83.8% of the initial sensitivity when its current density vs. time response was measured for 75 min in bare electrolytes prior to the glucose-sensing test. Furthermore, it demonstrated excellent repeatability performance by retaining 87.0% of the initial sensitivity when a single electrode was tested for 4 cycles. The proposed robust structured 3D SS-Co_3O_4 electrode successfully responds to the content of glucose in human saliva, which substantially proves its suitability in practical application. The synthesis technique is advantageous to prepare other metal oxides with interesting morphology and robust structure for the development of more reliable non-enzymatic glucometers and other electrochemical devices.

Keywords Straw-sheaf–like Co_3O_4 · Inert gas calcination · Non-enzymatic glucose detection · Chemically stable glucose sensor · Electrochemical biosensor

Introduction

To meet the increasing demands of point-of-care diagnostic procedures, a number of investigations have been conducted. These investigations focused on developing novel, simple, user-friendly, light-weight, portable, and cost-effective glucose sensors to ensure appropriate diabetes management and mitigate its adverse effects [1, 2]. To date, enzymatic sensors with fast response, good selectivity, and specificity are widely used in glucose monitoring [3, 4]. However, a series of accompanying problems owing to the intrinsic nature of the enzyme, such as it being easily affected by pH, temperature, and other environmental factors, should be taken into account [5]. Therefore, enzyme-less glucose sensors have attracted extensive attention due to its high repeatability and stability compared to enzymatic sensors, which have practical significance in both clinical diagnosis and food industries [6]. In relation to this, various metal oxides, such as CuO, Cu_2O, Co_3O_4, ZnO, NiO, MoO_3, MgO, and Fe_3O_4, play an important role in the development of high-performing non-enzymatic glucose sensors because the electrochemical performances of metal oxides can be regulated by tuning their morphology, surface area, and electronic properties [7–14].

Among various metal oxides, cobalt tetraoxide (Co_3O_4) is proven to be a suitable electrocatalyst for sensing because of its outstanding redox activity among the redox pairs, such as Co^{2+}/Co^{3+} and Co^{3+}/Co^{4+}. Furthermore, it is proven to be electrochemically stable, cheaper, and abundant in nature. Different Co_3O_4 nanostructures, including nanoflowers [15],

✉ Wanfeng Xie
wfxie@qdu.edu.cn

✉ Woochul Yang
wyang@dongguk.edu

[1] Department of Physics, Dongguk University, Seoul 04620, Republic of Korea

[2] College of Microtechnology & Nanotechnology, University-Industry Joint Center for Ocean Observation and Broadband Communication, Qingdao University, Qingdao 266071, China

nanosheets [16], and nanoflakes [17], are proved to be suitable for non-enzymatic glucose detection. As the nanostructure's characteristics reduce the diffusion paths for both electrons and ions, which in turn increases an interfacial redox reaction [18]. However, nanoscale building blocks generally tend to easily get damaged during the oxidation/reduction process due to their fragile nature, resulting in poor recyclability performance of the target electrochemical applications. Moreover, due to large interparticle resistance, nanoscale dimensions experience particle aggregation problems and weak electron transport networks simultaneously with electrocatalytic and electrochemical activities [19, 20]. Therefore, most of the reported works are based on composite materials, graphene-, polymer-, and other nanomaterial-based composites that are formed by utilizing expensive and toxic chemicals which are hazardous to the environment as well [21–24]. To overcome these challenges related to the nanoscale building blocks and composite structure of Co_3O_4, it is important to develop Co_3O_4 with microscale dimensions and robust structure. The former is advantageous in the case of long-range electron transport networks, while the latter results in excellent recyclability performance during the oxidation/reduction process. Furthermore, dual benefits from micro and nanoscale dimensions can be reaped in terms of reducing ion diffusion pathways and maximizing electrochemical reaction sites when primary nanoscale building blocks are integrated appropriately with secondary microscale dimensions. However, developing a micro- or nanoscale dimension with a robust structure that can efficiently conquer electrode-materials pulverization at the time of the oxidation/reduction process is still challenging. Thus, it is important to prepare Co_3O_4 with a robust structure as a high chemically stable electrode material with desirable characteristics such as high sensitivity that possesses high-quality sensing ability in glucose detection.

In the literature, researchers have developed an interesting structure called straw-sheaf (SS)–like structure with unique properties and validated its potential in different domains. For example, Bin et al. and Li et al. used cationic polymer adsorption as a charge-driven source and p-phthalic acid as a precipitator along with cobalt acetate, respectively, to prepare SS-Co_3O_4 as a high chemically stable material for LIB applications [20, 25]. Similarly, Wang et al. used the specific concentration of glycerin with sodium sulfate and calcium chloride to prepare SS-like α-calcium sulfate hemihydrate for water treatment [26]. Also, Shi et al. used the 1,2,4,5-benzenetetracarboxylic acid as an organic building block with terbium nitrate to construct SS-like terbium-based coordination polymer as selective luminescent probes for heavy metal ions [27]. These processes needed specific reagents with the base precursor for constructing SS-like morphology, hence making the process more complex and expensive. Furthermore, these specific reagents can influence the basic characteristics of the target material when annealing in air. For example, in the case of SS-Co_3O_4 preparation, these reagents and calcination treatment in air enlarge the diameter (~ 80–150 nm) of nanoneedles and expand the pore size (~ 2–40 nm), thereby minimizing the specific surface area (~ 16–28 $m^2.g^{-1}$), lowering the crystallinity, and increasing the charge transfer resistance (R_{ct} = ~ 20–80 Ω) at electrode/electrolyte interface [20, 25] because both entities (additional precursors and air molecules) can disturb the growth of hydrothermally produced nanoscale nuclei during the calcination treatment. Therefore, it is challenging to find a technique that is based on a single cobalt precursor and use a non-reactive gas environment instead of air for annealing to prepare SS-Co_3O_4 with a relatively large surface area, lower R_{ct} value, and high crystallinity.

In this study, we observed that using only inert gas for calcination treatment can be a simple alternative solution for the aforementioned challenges, such as avoiding the use of (i) additional precursors and (ii) calcination of hydrothermally produced cobalt nuclei in air. As inert gas helps to provide an O_2-free environment, thus, electrostatically grows the hydrothermally produced nuclei in nanowires orientation, while the calcination treatment self-assembles these nanoscale dimension's nuclei to form the secondary microscale dimensions with the SS-like morphology. Based on this idea, we successfully synthesized a high crystalline 3D SS-Co_3O_4 material with a large surface area (39.01 $m^2.g^{-1}$), smaller pore size (6 nm), and lower R_{ct} value (9.35 Ω). The prepared SS-Co_3O_4 is composed of nanoneedles ensuring the short diffusion pathway for fast electron transportation processes (R_{ct} = 9.35 Ω), enhancing the surface-reaction kinetics. Furthermore, the nanoneedles are strongly tied in the middle, guaranteeing the remarkable electrochemical stability of Co_3O_4. Based on these advantageous characteristics of SS-Co_3O_4, it demonstrated great potential in glucose-sensing applications.

Experimental section

Reagents and solutions

We procured cobalt (II) nitrate hexahydrate $Co(NO_3)_2{\cdot}6H_2O$, urea (CH_4N_2O), sodium hydroxide (NaOH) pellets, D-(+)-glucose, lactose, sucrose, mannose, maltose, ascorbic acid (AA), sodium chloride (NaCl), Polyvinylidene fluoride, SUPER C65 Nano Carbon Black, N-Methyl-2-Pyrrolidone (NMP), ethanol, and acetone from Sigma-Aldrich and used them without any purification.

Synthesis of SS-Co_3O_4

The $Co(NO_3)_2{\cdot}6H_2O$ of 0.73 g and CH_4N_2O of 0.66 g were dissolved in DI water (measuring 80 mL) and stirred for

approximately 1 h then the solution was transferred to a 100-mL Teflon-lined autoclave and the hydrothermal treatment was performed for 7.30 h at 110 °C. The solution was then allowed to cool naturally to room temperature and the red-colored paste was got in the product, which was dried at 80 °C in an oven for approximately 12 h. The obtained precursors were finally heated under argon (Ar) environment at a temperature of 430 °C for 3 h in a CVD furnace. The material, prepared as per the method detailed above, is called SS-Co_3O_4. A similar process was repeated to prepare SS-Co_3O_4 in nitrogen (N_2) and oxygen (O_2) environment. After the successful synthesis of SS-Co_3O_4, its morphological, structural, elemental, etc. analyses were characterized using various equipment, as discussed in the supplementary information (SI) sections.

Preparation of SS-Co_3O_4-based glucose electrode

To fabricate the electrodes, SS-Co_3O_4 as active materials was mixed with SUPER C65 carbon black and binder (PVDF) using NMP to produce a slurry. The uniform slurry obtained earlier was then coated on a carbon cloth electrode (CCE) and dried at a temperature of 100 °C for approximately 12 h.

Electrochemical studies of SS-Co_3O_4-based glucose electrode

The electrochemical response towards glucose (0.04 to 154.85 mM) detection was evaluated using a three-electrode system. The electrode based on Co_3O_4/CCE was used as a working electrode (WE), while the Pt wire was used as a counter electrode (CE) and Ag/AgCl was used as a reference electrode (RE). The fundamental informations, including the concentration of the stock solution, added volume from the stock solution to the electrolyte in each step, and related electrochemical discussion are provided in the SI section. Sensing analysis was performed using Linear Sweep Voltammetry (LSV) measurement at applied potential from 0 to 1 V in a NaOH solution at a constant concentration (1.0 M, pH 14). The linear fitted curve obtained between the maximum faradaic current density vs. various glucose concentrations was used to measure the sensor's sensitivity. In LSV curve, the maximum change in current density was obtained for glucose at + 0.48 V vs. Ag/AgCl in 1.0 M NaOH. Therefore, the amperometric J-T investigation were performed at + 0.48 V vs. Ag/AgCl in 1.0 M NaOH.

Results and discussion

Formation of SS-Co_3O_4

Schematic illustration (Fig. 1) shows that the SS-Co_3O_4 can be obtained via inert gas calcination treatment of hydrothermally produced nuclei. Figure 1a shows that both the precursors are decomposed to produce the cation (Co^{2+}), and anions (CO_3^{2-} and OH^-), where the cation leads to the formation of cobalt crystal nuclei over which the anions are physically adsorbed via electrostatic interaction, during the hydrothermal process. Nuclei growth can be tailored if annealed in different gasses, such as O_2, N_2, and Ar, environment because of heating in either the air or O_2, the oxygen gets adsorbed on the cation surface, disturbing the uniform distribution of the anions. Moreover, due to the higher electronegativity of O_2 molecules, it takes electrons from anions, thus reducing their concentrations. Therefore, the controlled crystal growth of these nuclei in an O_2 environment cannot be obtained and they require additional positively charged surfactants to compensate the role of negatively adsorbed O_2 molecules. Hence, Co_3O_4 calcinated in air demonstrated an irregular morphology as shown in Fig. SI 2 (a-f). Comparatively, inert gas calcination helps to retain the cations and anions with similar concentration and distribution as formed in the hydrothermal process, growing the nuclei in nanoneedles orientation as confirmed by the HRTEM (Fig. 1b). The HRTEM image (Fig. 1b) was taken for the product collected at the early stage of the calcination treatment (at 430 °C for 30 min) confirming that the nuclei are growing in a nanowire orientation. Furthermore, the HRTEM image (Fig. 1c)

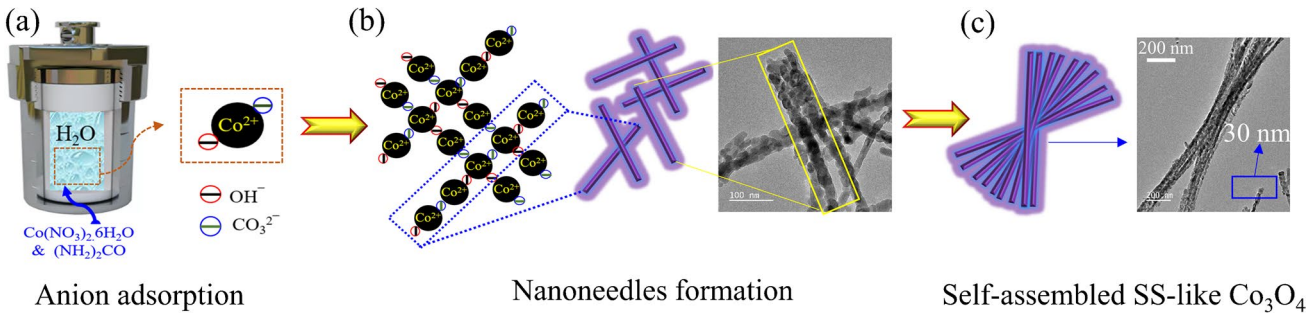

Fig. 1 Schematic illustration of the formation of 3D SS-Co_3O_4 and TEM images of the product taken at different stages of the reaction

of the final product indicated that 3 h calcination treatment self-assembled these nanowires by minimizing their surface energy and eventually forming the SS-like morphology of Co_3O_4 (Fig. 1c).

Morphological and structural analysis of SS-Co_3O_4

Figure 2a illustrates the FESEM image of the Co_3O_4 product, showing that it has a uniform SS-like architecture composed of nanoneedles, which are outspread and closely bound to each other in the middle to create this SS-like architecture. The length and average diameter of each nanowire are ~ 8 µm and ~ 30 nm, respectively. The SS-like architecture is favorable for the rapid electron transportation process, owing to the long-range pathway and reduced diffusion length of one-dimensional nanoneedles. Furthermore, nanoneedles that are strongly bound together in the middle position enable a robust structure that can withstand vigorous volume variations that occur as a result of repeated electrochemical reactions. Therefore, this SS-like network can overcome the challenges faced by Co_3O_4-based materials in terms of low sensitivity and low electrochemical stability toward glucose detection. Moreover, the microstructure of the SS-Co_3O_4 was investigated through HRTEM analysis, confirming a highly similar architecture to a bundle of straw as shown in Fig. 2b. Figure 2c shows that the nanowire's surface is mesoporous in nature, which is advantageous in generating additional active sites for enhanced surface reaction. Furthermore, the high-resolution image (Fig. 2e) of Fig. 2d confirms that the average diameter of each nanoneedle is approximately 30 nm. Moreover, Fig. 2f represents the d-spacing value of 0.24 nm confirming that the nanoneedles are grown in the (311) plane direction. The elemental composition of

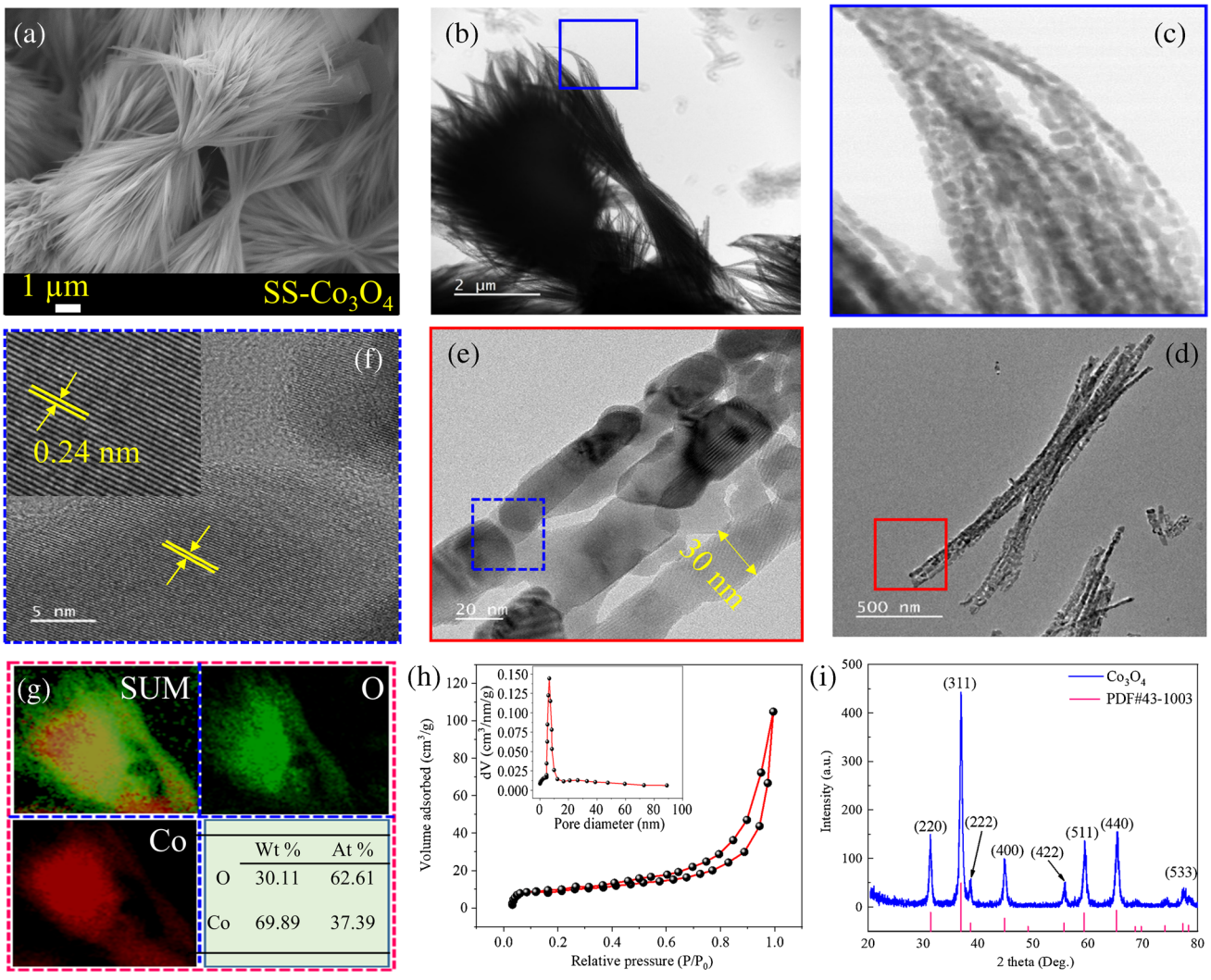

Fig. 2 **a** FESEM and **b–f** HRTEM images of 3D SS-Co_3O_4 calcinated in Ar environment. **g** EDS analysis of SS-Co_3O_4 to specify the existence of Co and O. **h** N_2 adsorption–desorption isotherm and **i** XRD pattern of SS-Co_3O_4

SS-Co_3O_4 was confirmed through the EDS analysis of Fig. 2b as shown in Fig. 2g. The Sum EDS image shows red and green color areas, indicating the existence of cobalt (Co) and oxygen (O) with wt. % of 69.89 and 30.11, respectively. Furthermore, Fig. SI1 (Supporting Information) shows the FESEM images of the SS-Co_3O_4 calcinated in the N_2 environment, while Fig. SI 2 (a-f) shows the FESEM images, EDS mapping, and spectrum of the Co_3O_4 samples calcinated in the air.

Moreover, the specific surface area and pore size of SS-Co_3O_4 were determined to be 39.01 $m^2 \cdot g^{-1}$ and 6.48 nm, respectively (Fig. 2h). The results show that the SS-Co_3O_4 exhibited a relatively high surface area along with numerous mesoporous on nanoneedles surfaces. Furthermore, Fig. 2i shows that the XRD analysis was conducted to examine the structural characteristics of SS-Co_3O_4. The diffraction peaks originated at $2\theta = 31.6°$, 36.8°, 44.8°, 59.3°, and 65.2° are corresponded to (220), (311), (400), (511), and (440) crystal planes of face-centered cubic phase of Co_3O_4 (JCPD#43–1003) [28, 29]. The peak for the (311) plane had a higher intensity than the other peaks, indicating that the nanoneedles of SS-Co_3O_4 are mainly grown in the 311-plane direction. In addition, no extra peaks were found in XRD results, indicating that SS-Co_3O_4 was synthesized without any impurities.

Glucose-sensing performances of SS-Co_3O_4

After the UV–Vis spectroscopy, electrochemical, chemical structure, and surface analysis of SS-Co_3O_4, as discussed in the SI sections, its sensing performance was carried out by measuring the LSV response with the step-wise addition of glucose. Figure 3a shows the LSV response of SS-Co_3O_4 towards various concentrations of glucose, showing a rapid increase in the anodic peak of the current density when the concentration of glucose changed from 0.04 to 124 mM. Figure 3b shows that the anodic peak of current density increased linearly in the range from 0.04 to 4.85 mM. The regression equation $J_{pa}(mA.cm^{-2}) = 0.6699x + 0.1239c_{glucose}$ (mM) with correlation coefficient ($R^2 = 0.997$) for the linear range of 0.04 to 4.85 mM was used to determine the slope of the calibration plot, which defines the sensitivity 669 $\mu A.mM^{-1}\ cm^{-2}$ of the sensor [30, 31]. The limit of detection (LOD) was determined to be 0.31 µM using the equation: $LOD = 3.3 \times (\sigma/S)$, where σ represents the standard error of the intercept, while S represents the slope of the linear fitted curve [32, 33].

The electro-oxidation performances of SS-Co_3O_4-based electrodes towards glucose detection were further examined by recording amperometric J-T curves as shown in Fig. 3c. These experiments were conducted with nonstop stirring and stepwise addition of glucose at + 0.48 V, in 1.0 M NaOH. The linear fitted plot of Fig. 3c is derived as shown in Fig. 3d, which also demonstrates a linear relationship between the changes in current density with glucose concentration that ranged between 0.04 and 4.85 mM. In this measurement, the sensitivity, R^2, and LOD were determined to be 635 $\mu A.mM^{-1}\ cm^{-2}$, 0.989, and 0.32 µM, correspondingly.

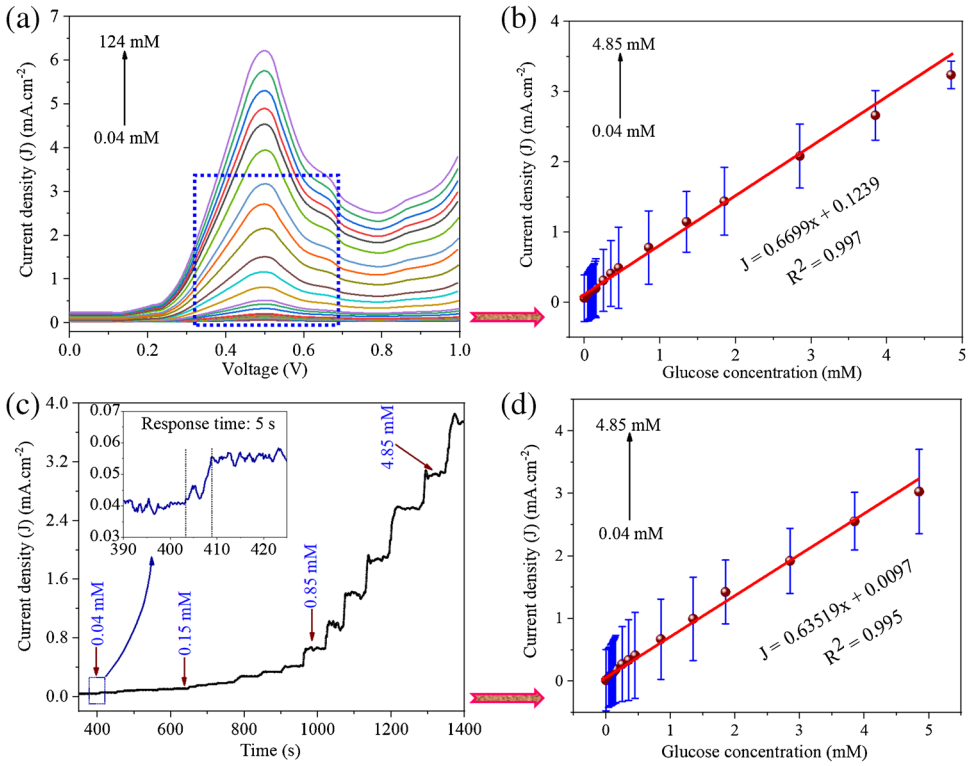

Fig. 3 **a** LSV and **c** J-T response of Co_3O_4-based electrode and their corresponding linear fitted plots, where the error bars show RSD of **b** 0.92% for n = 3 and **d** 1.17% for n = 3, respectively, used for sensitivity and linear response range determination. The inset plot in **c** shows the sensor response time

Furthermore, the response time, the time taken by the signal to reach 90% of the equilibrium value, while changing the concentration of glucose in the electrolyte [34, 35], was determined to be between 5 s as shown in the inset plot of Fig. 3c. Figure SI 6 (a, c) is an illustration of the variation in response of current density obtained by either LSV or J-T measurement towards glucose concentrations ranging from 0.04 to 124 mM. The change in current density vs. glucose concentration plots (Fig. SI 6 (b, d)) of Fig. SI 6 (a, c) showed that there was a significant reduction observed in the slope of the fitting curve at more than 4.85 mM concentration. This infers a weak sensitivity of sensing electrodes in case of a high concentration of glucose. This can be attributed to the presence of varying electrochemical kinetics. In case of an increase in the concentration of glucose in an alkaline solution, a gradual increase in glucose diffusion rate can be observed. It then goes beyond the consumption rate at the electrode surface, resulting in a gradual saturation of the electrochemical reaction rate in line with the charge flow rate making it impossible for the response current density to increase linearly at a high concentration. Therefore, it can be concluded that the synthesis of sensing electrodes with a high surface-to-volume ratio remains an important parameter in producing high-performing non-enzymatic glucose sensors. For comparative purposes, Table 1 tabulates the value of a few important parameters, such as LOD sensitivity, response time, and analytical range in line with Co_3O_4-related electrode materials. The table values infer that the glucose sensor based on 3D SS-Co_3O_4 demonstrates a relatively high performance to glucose compared to all other sensors reported previously. These excellent performances of SS-Co_3O_4-based electrodes can be attributed to a unique 3D SS-like structure with a relatively high surface-to-volume ratio and the presence of numerous nanoporous on nanoneedles surfaces. These characteristics are beneficial for the enhanced surface reaction kinetics and lowered charge transfer resistance for the fast flow of electrons and ions at the electrode/electrolyte interface.

Selectivity, reproducibility, repeatability, chemical stability, and real-time analysis of SS-Co_3O_4

Anti-interference capacity (selectivity), reproducibility, repeatability, and chemical stability are critical parameters to be determined for the validation of any glucose-sensing electrode. Therefore, the study was extended to determine these parameters for the SS-Co_3O_4-based electrode. The selectivity of Co_3O_4 (Fig. 4a) was analyzed by adding 0.35 mM concentrations of various interfering substances such as lactose, sucrose, mannose, maltose, AA, and NaCl, with 0.25 mM concentrations of glucose to the electrolyte at different stages of the test. The result shows that each interfering substance leaves behind 70% smaller changes in response to current density, recorded against 0.35 mM concentration when compared to the current density response value during the addition of 0.25 mM glucose. Therefore, the developed non-enzymatic SS-Co_3O_4-based electrode exhibits good selectivity in detecting the actual glucose.

Moreover, the reproducibility analysis (Fig. 4b) was conducted through amperometric response of six different SS-Co_3O_4-based electrodes as shown in Fig. SI 6–9 and discussed in the SI-section. The RSD value of the sensitivity of six electrodes was determined to be 2.25% (Fig. 4b), suggesting excellent reproducibility and precision of SS-Co_3O_4-based electrode for glucose detection. In addition, the anti-interference capacity of each electrode was analyzed under similar test conditions and utilized for amperometric (J-T) curves as shown in subfigure (d) of Fig. SI 6–9. The result shows that the interference from each of the interfering substances towards glucose detections is almost negligible.

The reusability analysis was conducted by measuring the J-T response of a single electrode at various concentrations

Table 1 Analytical performance comparison of SS-Co_3O_4-based glucose sensor with those reported previously

Sample	Linear range (mM)	Sensitivity ($\mu A.mM^{-1}.cm^{-2}$)	Detection limit (μM)	Response time (s)	Ref
SS-Co_3O_4	0.04–4.85	669	0.31	~5	This study
Co_3O_4/3D-KSCs	0.088–7	1377	26	–	[45]
Co_3O_4/Zn	0.005–0.62	193	2.0	<7	[46]
ZIF-67 derived Co_3O_4	1.5–10.5	50	–	4	[47]
porous Co_3O_4	0–0.8	1060.1	0.32	–	[48]
Co3O4/graphene	0.001–9	214	0.41	0.49	[49]
NHCN-Co_3O_4	0.001–32	12.9	0.2	-	[50]
Co_3O_4 nanosheets	Up to 0.31	12,970	0.058	<10	[51]
Nest-like Co_3O_4	0.02–0.4	929	1.0	0.5	[52]
TiO_2/Co_3O_4 ANTAs	0.01–3.0	2008.82	0.3396	<5	[53]
Co_3O_4 @graphene	0.02–8	628	0.038	4	[54]

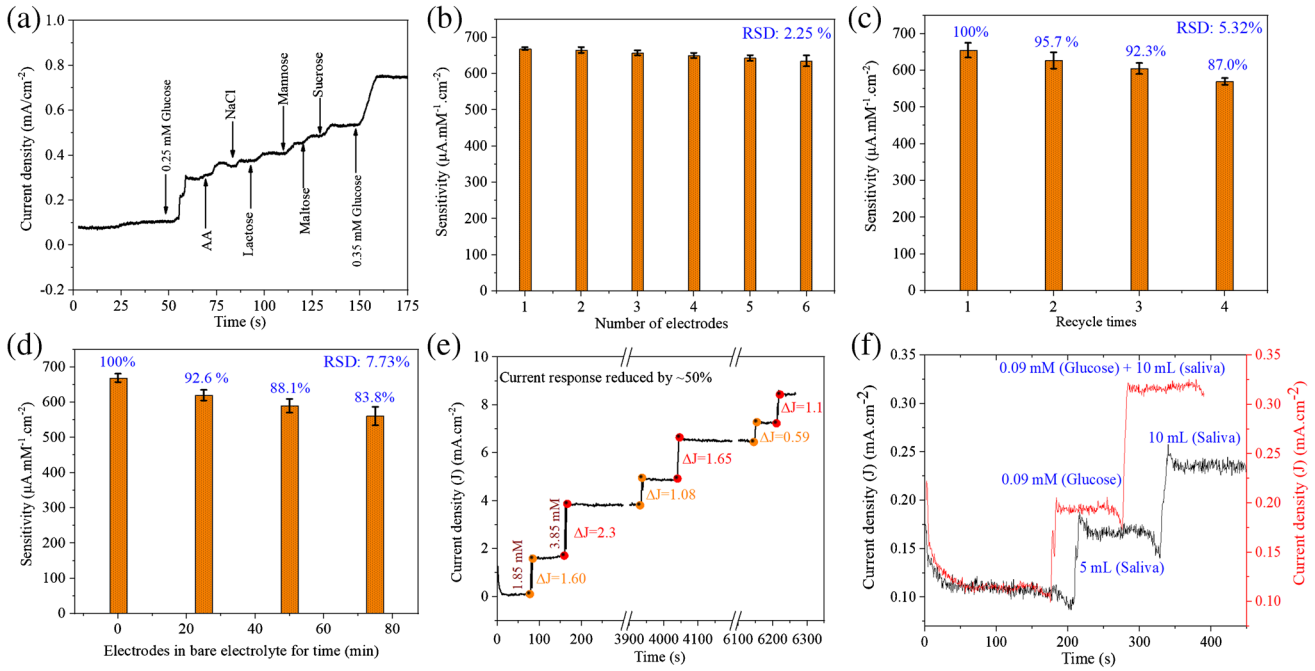

Fig. 4 **a** Selectivity, **b** reproducibility, **c** repeatability, **d** chemical stability, **e** continuous measurement of 1.85 and 3.85 mM concentrated glucose for 105 min, and **f** real-sample analysis of SS-Co_3O_4-based glucose-sensing electrode

ranging from 0.04 to 4.85 mM four times. The RSD value was determined to be 5.32% as shown in Fig. 4c, demonstrating excellent repeatability. Also, the electrodes measured in the 4th cycle retained 87.0% of their initial sensitivity and reduced the linearity to 0.963, confirming the excellent reusability performance of the SS-Co_3O_4-based electrode. Figures SI 10 (a-d) and 11 (a-d) illustrate the raw-data plots that corresponded to repeatability analysis. Lastly, the chemical stability of SS-Co_3O_4 was also investigated as shown in Fig. 4d. The procedures used for chemical stability investigation are discussed in the SI section and Fig. SI 12 (a-i) illustrates the corresponding raw-data plots. The RSD value was determined to be 7.73% as shown in Fig. 4d. The electrodes measured for 75 min in the bare electrolyte retained 83.8% of its initial sensitivity and reduced the linearity to 0.964, confirming the excellent chemical stability performance of the SS-Co_3O_4-based electrode. Moreover, it is a fact that the long runs of glucose measurements generate gluconolactone or other products derived from the electrocatalytic oxidation of glucose, which deposits onto the electrode surface and further shield the electrocatalytic sites of these metal oxides. In this sense, a quick decay of the analytical performance of the non-enzymatic glucose sensors can be observed. Therefore, the stability analysis in terms of continuous measurement of glucose was further confirmed by measuring the J-T analysis for a longer time ~ 105 min, as shown in Fig. 4e. This analysis was performed by spiking 1.85 and 3.85 mM concentrated glucose at different stages of the analysis. The result (Fig. 4e) revealed that the SS-Co_3O_4-based electrode retained around ~ 50% of its initial current density response to each concentration. These excellent stability analyses are attributed to the robust structure of Co_3O_4 that can efficiently conquer electrode-materials pulverization at the time of the oxidation/reduction process.

Furthermore, the study was extended to the detection of glucose in saliva samples of human subjects. As Fig. 3b, d reveals, the current jumps upon the addition of a sufficiently low concentration of glucose from 40 to 150 μM, which is comparable to the glucose concentration of saliva (20 − 210 μM) found in normal individuals and diabetes patients [36, 37]. Moreover, the LOD of our constructed electrode is 0.31 μM; therefore, it can be worked for non-invasive glucose sensing using human fluids. For this analysis, the saliva samples were collected from human subjects and centrifuged at 5000 rpm for 6 min, then around 5 mL saliva supernatant is added to 30 mL of 1.0 M NaOH, and the amperometry of this solution was performed at + 0.48 V vs. Ag/AgCl (Fig. 4f). The current density difference was obtained to be 0.06 mA.cm^{-2} than the initial value, which is almost equivalent to the current density response obtained when the 0.07 mM concentration of glucose was spiked to the 30 mL NaOH. Moreover, Fig. 4f shows the comparative response of glucose detection when bare 0.09 mM glucose and 10 mL saliva sample mixed with the 0.09 mM glucose were added to the electrolyte. Interestingly, a greater change in current density was obtained for the mixed glucose

and saliva sample than that of the bare 0.09 mM glucose, confirming the response of the SS-Co_3O_4-based electrode towards the amount of glucose in saliva, therefore generating a higher current signal.

Glucose-sensing mechanism

The conduction band (E_{CB}), valence band (E_{VB}), and Fermi level (E_F) positions are important components to consider when investigating the glucose-sensing process of SS-Co_3O_4 because the difference between the E_F and electrolyte oxidation potential (E_{EOP}) determines the Schottky barrier height (ϕ_B) and the overpotential requires to flat the bands of semiconductor with the E_{EOP} for the migration of charge at electrode/electrolyte interface [38–40]. In addition, it is also important to consider a semiconductor if it exhibited more negative and more positive band edge potential of E_{CB} and E_{VB} than the potential required for $\bullet O_2^-$ and OH^- radicle generation for electrochemical-based application [41] because in the electrochemical reaction, the bare electrolyte initially interacts with the semiconductor generating $\bullet O_2^-$ and OH^-, which form the Inner Helmholtz layer (IHL) with a semiconductor surface (double-layer capacitance). Later, when the target analyte (glucose in our case) is added to the electrolyte, it forms the outer Helmholtz layer (OHL). Thus, if a semiconductor has better activity towards $\bullet O_2^-$ and OH^-, radicles generation (particularly OH^- radicles) can excellently oxidize glucose.

Therefore, the E_{CB}, E_{VB}, E_F, R_{ct}, and band gap energy (E_g) were determined by performing VB XPS, M-S plot, EIS, and tauc plot measurements. Figure 5a and its inset figure indicate the VB XPS potential and tauc plot analysis, confirming that SS-Co_3O_4 exhibited a VB potential and E_g of 0.56 eV and 2.16 eV, respectively. The M – S plot (Fig. 5b) was constructed at different frequencies such as 100 Hz, 316 Hz, and 1 kHz, which indicates the negative slope, confirming the p-type nature of SS-Co_3O_4 [42]. The E_{FB} value was determined to be 0.88 eV through extrapolation of the linear region of capacitance to intersect at the potential axis. Moreover, EIS analysis of the SS-Co_3O_4-based electrode was performed to analyze interfacial reaction processes as well as catalytic kinetics between electrode and electrolyte (Fig. 5c). The fitting was performed on the radius of the semicircle area in Nyquist plots and the R_{ct} value was determined to be 9.35 Ω (shown in the inset of Fig. 5c) based on the equivalent circuit sketched in Fig. 5c. The least R_{ct} value infers that the nanoneedles can reduce the ion diffusion pathways and promote the charge transfer process across the electrode–electrolyte junction. Lastly, the energy band diagram of SS-Co_3O_4 was illustrated as shown in Fig. 5d, confirming that Co_3O_4 exhibits more negative and more positive band edge potential of

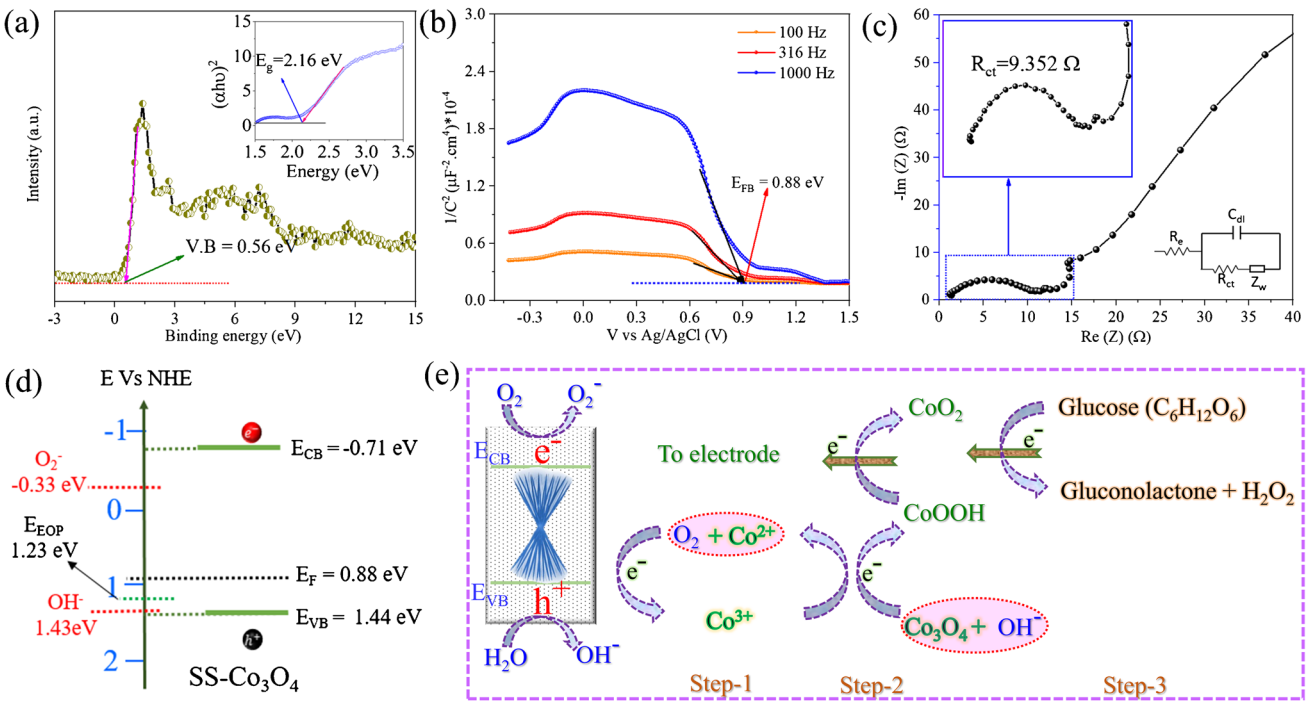

Fig. 5 **a** Valance band spectra and its inset show the tauc plot of SS-Co_3O_4. **b** M-S plot and **c** EIS analysis of SS-Co_3O_4. The inset equivalent circuit in **c** was obtained through fitting the EIS data, where C_{dl}, R_e, R_{ct}, and Z_w are corresponded to the double-layer capacitance, electrolyte, charge transfer, and Warburg resistance, respectively. **d** Schematic illustration of energy bands of SS-Co_3O_4 and **e** the process involved in the glucose-sensing mechanism

E_{CB} and E_{VB} than the potential required for $\bullet O_2^-$ and OH^- radicle generation, respectively; therefore, SS-Co_3O_4 can excellently generate these radicles in the initial electrochemical reaction that takes place between SS-Co_3O_4 and the bare electrolyte. However, the valance edge potential (1.46 eV) of Co_3O_4 typically has a smaller difference (0.03 eV) than the potential of OH^- (1.44 eV at pH > 13 [43]), therefore demonstrating a poor electrochemical activity. Tuning the surface and morphology of the Co_3O_4 is an effective way to override this challenge because the large surface area reduces the diffusion paths both for electrons and ions, which in turn increases an interfacial redox reaction. In this regard, the developed SS-like structure is advantageous because it exhibited a relatively high surface area as well as numerous mesoporous on nanoneedles surfaces that generate additional active sites for enhanced surface reaction kinetics than previous Co_3O_4-based studies listed in Table 1.

Figure 5e illustrates the glucose-sensing mechanism, where SS-Co_3O_4 was employed as glucose oxidizing electrodes. The sensing process shows that the electrons in the E_{CB} of the Co_3O_4 are responsible for the reduction of O_2 molecules by oxidizing Co^{2+} to Co^{3+} (Eq-SI1 and -SI2) and the holes in its E_{VB} are responsible for the generation of OH^- (Eq-SI3). The produced OH^- radicles react with Co_3O_4 to generate CoOOH species and release an electron, reverting the Co^{3+} to Co^{2+} (Eq-SI4 and SI-5) [44]. The reaction between CoOOH and the OH^- (from NaOH electrolyte) takes place producing CoO_2 species, H_2O molecules, and an electron (Eq-SI6). Secondly, when glucose is added, the glucose molecules ($C_6H_{12}O_6$) are catalytically oxidized by CoO_2 species to gluconolactone ($C_6H_{10}O_6$) and H_2O_2 (Eq-SI7). Lastly, H_2O_2 oxidizes to produce H_2O molecules and O_2 molecules and release two electrons (Eq-SI8). The released electrons are transferred to the circuit through the E_{CB}, thus increasing the current density of the oxidation peak, while the O_2 molecules restart the process (Eq-SI1). More $\bullet O_2^-$ and OH^- radicles are generated due to enhanced surface reaction of kinetics, thus enabling SS-Co_3O_4 to oxidize more glucose molecules, while more electrons are rapidly transferred from the electrolyte to SS-Co_3O_4 due to the lower value of R_{ct}. Similarly, it provides long-range electron transport networks for easy transportation of electrons to the current collector electrode due to the nanoneedle-like morphology of SS-Co_3O_4, thus enhancing the current density linearly as the glucose concentration increases. Therefore, SS-Co_3O_4-based electrode demonstrates a high glucose sensitivity, broader linear range, low LOD, and fast response time.

Conclusion

In this work, a nanozyme of Co_3O_4 was developed via inert gas calcination treatment of hydrothermally produced cobalt nuclei. A simple, efficient, inexpensive, and self-driven method was approached to produce the demanded SS-like structure of Co_3O_4. Based on the robust structure and enhanced surface area of the SS-Co_3O_4-based electrode, it demonstrated a better sensitivity, fast response, wide linear range, high chemical stability, low detection limit, good selectivity, outstanding reproducibility, and repeatability capability for glucose detection. The successful response towards the content of glucose in human saliva substantially proves its suitability in practical application. The synthesis techniques can offer a new strategy for preparing metal oxides with interesting morphology and robust structure, which can be employed in fabricating enzymeless sensors for detecting biomolecules. Although the obtained results are very interesting. However, our sensing setup still places certain limits on the size and testing volume. Therefore, in near future, we are planning to design sensor chips for real-time measurements. As the sensor chip is advantageous for the detection of analytes in wide linear ranges, which does not require sample dilution, thus making it ideal for clinical applications such as blood-based analyte measurements.

Supplementary Information The online version contains supplementary material available at https://doi.org/10.1007/s00604-022-05453-9.

Acknowledgements This research was supported by the Brain Pool program funded by the Ministry of Science and ICT Education and by Basic Science Research Program through the National Research Foundation of Korea (Nos. 2020H1D3A1A04081310, 2021R1I1A1A01056213, 2021H1D3A2A01100019, and 2019R1A2C1002844).

Declarations

Conflict of interest The authors declare no competing interests.

References

1. Umapathi R, Ghoreishian SM, Sonwal S, Rani GM, Huh YS (2022) Portable electrochemical sensing methodologies for on-site detection of pesticide residues in fruits and vegetables. Coord Chem Rev 453:214305
2. Wang Y, Haick, Guo S, Wang C, Lee S, Yokota T et al (2022) Skin bioelectronics towards long-term, continuous health monitoring. Chem Soc Rev
3. Reddy VS, Agarwal B, Ye Z, Zhang C, Roy K, Chinnappan A et al (2022) Recent advancement in biofluid-based glucose sensors using invasive, minimally invasive, and non-invasive technologies: a review. Nanomaterials 12:1082
4. Khor SM, Choi J, Won P, Ko SH (2022) Challenges and strategies in developing an enzymatic wearable sweat glucose biosensor as a practical point-of-care monitoring tool for type II diabetes. Nanomaterials 12:221
5. Giovannini G, Cinelli P, Boesel LF, Rossi RM (2022) Thioflavin-modified molecularly imprinted hydrogel for fluorescent-based non-enzymatic glucose detection in wound exudate. Materials Today Bio 14:100258
6. Xu Y, Zhao J, Qin L, Tang X, Wu B, Xiang Y (2022) Synthesis of CoNi2S4 nanoflake-modified nickel wire electrode for sensitive non-enzymatic detection of glucose. Sens Actuators Rep 100090

7. Chang H-W, Chen S-C, Chen P-W, Liu F-J, Tsai Y-C (2022) Constructing morphologically tunable copper oxide-based nanomaterials on Cu wire with/without the deposition of manganese oxide as bifunctional materials for glucose sensing and supercapacitors. Int J Mol Sci 23:3299
8. Asif M, Haitao W, Shuang D, Aziz A, Zhang G, Xiao F et al (2017) Metal oxide intercalated layered double hydroxide nanosphere: with enhanced electrocatalyic activity towards H2O2 for biological applications. Sens Actuators, B Chem 239:243–252
9. Asif M, Aziz A, Ashraf G, Wang Z, Wang J, Azeem M et al (2018) Facet-inspired core–shell gold nanoislands on metal oxide octadecahedral heterostructures: high sensing performance toward sulfide in biotic fluids. ACS Appl Mater Interfaces 10:36675–36685
10. Vignesh A, Vajeeston P, Pannipara M, Al-Sehemi AG, Xia Y (2022) Bimetallic metal-organic framework derived 3D hierarchical NiO/Co3O4/C hollow microspheres on biodegradable garbage bag for sensitive, selective, and flexible enzyme-free electrochemical glucose detection. Chem Eng J 430:133157
11. Zhou F, Li Y, Tang Y, Gao F, Jing W, Du Y et al (2022) A novel flexible non-enzymatic electrochemical glucose sensor of excellent performance with ZnO nanorods modified on stainless steel wire sieve and stimulated via UV irradiation. Ceram Int 48:14395–14405
12. Salarizadeh N, Habibi-Rezaei M, Zargar SJ (2022) NiO–MoO3 nanocomposite: a sensitive non-enzymatic sensor for glucose and urea monitoring. Mater Chem Phys 281:125870
13. Ullah H, Ahmad R, Khan AA, Khaliq N, Khan M, Ali G et al (2022) A sensitive non-enzymatic glucose sensor based on MgO entangled nanosheets decorated with CdS nanoparticles: experimental and DFT study. J Mol Liq 119366
14. Asif M, Liu H, Aziz A, Wang H, Wang Z, Ajmal M et al (2017) Core-shell iron oxide-layered double hydroxide: high electrochemical sensing performance of H2O2 biomarker in live cancer cells with plasma therapeutics. Biosens Bioelectron 97:352–359
15. Mondal S, Madhuri R, Sharma PK (2017) Probing the shape-specific electrochemical properties of cobalt oxide nanostructures for their application as selective and sensitive non-enzymatic glucose sensors. Journal of Materials Chemistry C 5:6497–6505
16. Mahmoudian M, Basirun W, Woi PM, Sookhakian M, Yousefi R, Ghadimi H et al (2016) Synthesis and characterization of Co3O4 ultra-nanosheets and Co3O4 ultra-nanosheet-Ni (OH) 2 as non-enzymatic electrochemical sensors for glucose detection. Mater Sci Eng C 59:500–508
17. Soomro RA, Ibupoto ZH, Sherazi STH, Abro MI, Willander M, Mahesar SA et al (2015) Glycine-assisted preparation of Co3O4 nanoflakes with enhanced performance for non-enzymatic glucose sensing. Mater Express 5:437–444
18. Zhang W, Jia G, Li H, Liu S, Yuan C, Bai Y et al (2016) Morphology-modulated mesoporous CuO electrodes for efficient interfacial contact in nonenzymatic glucose sensors and high-performance supercapacitors. J Electrochem Soc 164:B40
19. Sun Y, Liu N, Cui Y (2016) Promises and challenges of nanomaterials for lithium-based rechargeable batteries, Nature. Energy 1:1–12
20. Wang B, Lu X-Y, Tsang C-W, Wang Y, Au WK, Guo H et al (2018) Charge-driven self-assembly synthesis of straw-sheaf-like Co3O4 with superior cyclability and rate capability for lithium-ion batteries. Chem Eng J 338:278–286
21. Wang X, Dong X, Wen Y, Li C, Xiong Q, Chen P (2012) A graphene–cobalt oxide based needle electrode for non-enzymatic glucose detection in micro-droplets. Chem Commun 48:6490–6492
22. Jo HJ, Shit A, Jhon HS, Park SY (2020) Highly sensitive non-enzymatic wireless glucose sensor based on Ni–Co oxide nanoneedle-anchored polymer dots. J Ind Eng Chem 89:485–493
23. Zhang C, Ren J, Xing Y, Cui M, Li N, Liu P et al (2020) Fabrication of hollow ZnO-Co3O4 nanocomposite derived from bimetallic-organic frameworks capped with Pd nanoparticles and MWCNTs for highly sensitive detection of tanshinol drug. Mater Sci Eng C 108:110214
24. Chang AS, Tahira A, Solangi ZA, Solangi AG, Ibupoto MH, Chang F et al (2022) Pd-Co3O4-based nanostructures for the development of enzyme-free glucose sensor. Bull Mater Sci 45:1–9
25. Li L, Dai J, Jiang G, Sun X, Huang Z, Xie Z et al (2019) Three-dimensional mesoporous straw-like Co3O4 anode with enhanced electrochemical performance for lithium-ion batteries. ChemistrySelect 4:6879–6885
26. Zhang G, Cao D, Wang X, Guo S, Yang Z, Cui P et al (2022) α-calcium sulfate hemihydrate with a 3D hierarchical straw-sheaf morphology for use as a remove Pb2+ adsorbent. Chemosphere 287:132025
27. Shi M, Zeng C, Wang L, Nie Z, Zhao Y, Zhong S (2015) Straw-sheaf-like terbium-based coordination polymer architectures: microwave-assisted synthesis and their application as selective luminescent probes for heavy metal ions. New J Chem 39:2973–2979
28. Han D, Ma X, Yang X, Xiao M, Sun H, Ma L et al (2021) Metal organic framework-templated fabrication of exposed surface defect-enriched Co3O4 catalysts for efficient toluene oxidation. J Colloid Interface Sci 603:695–705
29. Chen J, Zhang L, Sun J, Zhu J, Wang X, Fu Y (2022) The construction of hierarchical hollow double-shelled Co3O4 for the enhanced thermal decomposition of ammonium perchlorate. Appl Surf Sci 571:151342
30. Ahmed J, Rashed MA, Faisal M, Harraz FA, Jalalah M, Alsareii S (2021) Novel SWCNTs-mesoporous silicon nanocomposite as efficient non-enzymatic glucose biosensor. Appl Surf Sci 552:149477
31. Meng T, Shang N, Zhao J, Su M, Wang C, Zhang Y (2021) Facile one-pot synthesis of Co coordination polymer spheres doped macroporous carbon and its application for electrocatalytic oxidation of glucose. J Colloid Interface Sci 589:135–146
32. Huang X-Y, Chi Z-T, Liu J, Li D-H, Sun X-J, Yan C et al (2020) Enhanced gas sensing performance based on p-NiS/n-In2O3 heterojunction nanocomposites. Sens Actuators, B Chem 304:127305
33. Huang XY, Chi ZT, Yang W, Deng Y, Xie WF (2022) Synthesis of Bi2O2CO3/In (OH) 3 xH2O nanocomposites for isopropanol sensor with excellent performances at low temperature. Sens Actuators B Chem 131715
34. Hilal M, Yang W (2022) A dual-functional flexible sensor based on defects-free Co-doped ZnO nanorods decorated with CoO clusters towards pH and glucose monitoring of fruit juices and human fluids, Nano. Convergence 9:1–17
35. Yao Y, Chen J, Guo Y, Lv T, Chen Z, Li N et al (2021) Integration of interstitial fluid extraction and glucose detection in one device for wearable non-invasive blood glucose sensors. Biosens Bioelectron 179:113078
36. Jurysta C, Bulur N, Oguzhan B, Satman I, Yilmaz TM, Malaisse WJ et al (2009) Salivary glucose concentration and excretion in normal and diabetic subjects. J Biomed Biotechnol
37. Gao W, Zhou X, Heinig NF, Thomas JP, Zhang L, Leung KT (2021) Nonenzymatic saliva-range glucose sensing using electrodeposited cuprous oxide nanocubes on a graphene strip. ACS Applied Nano Materials 4:4790–4799
38. Krol RVD (2012) Principles of photoelectrochemical cells, Photoelectrochemical hydrogen production. Springer. pp 13–67
39. Cong Y, Zhang J, Chen F, Anpo M, He D (2007) Preparation, photocatalytic activity, and mechanism of nano-TiO2 co-doped with nitrogen and iron (III). The Journal of Physical Chemistry C 111:10618–10623

40. Liu Y, Kang Z, Zhang S, Li Y, Wu H, Wu J et al (2018) Ferroelectric polarization-enhanced charge separation in a vanadium-doped ZnO photoelectrochemical system, Inorganic Chemistry. Frontiers 5:1533–1539
41. Xu Y, Liu Q, Liu C, Zhai Y, Xie M, Huang L et al (2018) Visible-light-driven Ag/AgBr/ZnFe2O4 composites with excellent photocatalytic activity for E. coli disinfection and organic pollutant degradation. J colloid Interface Sci 512:555–66
42. Bao E-P, Dong R, Zhang S, Li H, Zhang W, Zou J et al (2021) A tubular g-C3N4 based composite photocatalyst combined with Co3O4 nanoparticles for photocatalytic degradation of diesel oil. Catal Lett 151:3437–3450
43. Nosaka Y, Nosaka AY (2017) Generation and detection of reactive oxygen species in photocatalysis. Chem Rev 117:11302–11336
44. Turkkan G, Bas SZ, Atacan K, Ozmen M (2022) An electrochemical sensor based on a Co 3 O 4–ERGO nanocomposite modified screen-printed electrode for detection of uric acid in artificial saliva. Anal Methods 14:67–75
45. Wang L, Zhang Y, Xie Y, Yu J, Yang H, Miao L et al (2017) Three-dimensional macroporous carbon/hierarchical Co3O4 nanoclusters for nonenzymatic electrochemical glucose sensor. Appl Surf Sci 402:47–52
46. Chowdhury M, Cummings F, Kebede M, Fester V (2017) Binderless solution processed Zn doped Co3O4 film on FTO for rapid and selective non-enzymatic glucose detection. Electroanalysis 29:578–586
47. Kuppuswamy GP, Pushparaj K, Surya VJ, Varadharaj EK, Kumar SS, Di Natale C et al (2022) A ZIF-67 derived Co 3 O 4 dodecahedron shaped microparticle electrode based extended gate field-effect transistor for non-enzymatic glucose detection towards the diagnosis of diabetes mellitus. J Mater Chem C
48. Xiao X, Zhang Z, Li J, Nan F, Li Y, Wang Y (2021) High-performance non-enzymatic glucose sensors based on porous Co3O4 synthesized by coprecipitation method with the different precipitants. Ionics 27:1803–1812
49. Zhao J, Zheng C, Gao J, Gui J, Deng L, Wang Y et al (2021) Co3O4 nanoparticles embedded in laser-induced graphene for a flexible and highly sensitive enzyme-free glucose biosensor. Sens Actuators, B Chem 347:130653
50. Ouyang Y, Zheng X, Li Q, Ye N, Mo G (2022) ZIFs derived polyhedron with cobalt oxide nanoparticles as novel nanozyme for the biomimetic catalytic oxidation of glucose and non-enzymatic sensor. Anal Chim Acta 1209:339839
51. Meng S, Wu M, Wang Q, Dai Z, Si W, Huang W et al (2016) Cobalt oxide nanosheets wrapped onto nickel foam for non-enzymatic detection of glucose. Nanotechnology 27:344001
52. Rajeshkhanna G, Umeshbabu E, Rao GR (2017) Charge storage, electrocatalytic and sensing activities of nest-like nanostructured Co3O4. J Colloid Interface Sci 487:20–30
53. Gao Z, Zhang L, Ma C, Zhou Q, Tang Y, Tu Z et al (2016) TiO2 decorated Co3O4 acicular nanotube arrays and its application as a non-enzymatic glucose sensor. Biosens Bioelectron 80:511–518
54. Yang M, Jeong J-M, Lee KG, Lee SJ, Choi BG (2017) Hierarchical porous microspheres of the Co3O4@ graphene with enhanced electrocatalytic performance for electrochemical biosensors. Biosens Bioelectron 89:612–619